

RECENT IMPROVEMENTS IN THE FABRICATION AND PERFORMANCES OF AlN BASED PIEZOELECTRIC VIBRATION ENERGY HARVESTERS

M. Renaud*, R. Elfrink, M. Jambunathan, C. de Nooijer, M. Rovers, R. Vullers and R. van Schaijk
¹Imec/Holst Centre, Eindhoven, the Netherlands
*Presenting Author: Michael.Renaud@imec-nl.nl

Abstract: Piezoelectric vibration energy harvesters (PVEH) represent an advantageous alternative to electrochemical batteries traditionally used for powering wireless sensor nodes. MEMS technologies allow low cost manufacturing of PVEH when large scale production is considered. Therefore, we developed MEMS fabricated PVEH based on CMOS compatible Aluminum Nitride (AlN) as piezoelectric material. Recent improvements related to two aspects of these devices are presented: better reliability of the fabrication process and higher power generation thanks to reduced parasitic losses and to a thicker piezoelectric layer. The presented PVEH allows generating up to 450 μW for a footprint of about 1 cm^2 .

Keywords: piezoelectric, mechanical vibrations, MEMS

INTRODUCTION

Recently, wireless sensor networks paved the way for a large panel of applications [1]. Harvesting energy from environmental mechanical vibrations is a promising alternative to electrochemical batteries for supplying electrical power to the wireless nodes.

MEMS vibration energy harvesters (PVEH) based on the piezoelectric effect were developed by our team [2]. As illustrated by Fig. 1, they consist of a silicon cantilever attached to a proof mass and supporting a piezoelectric capacitor. AlN is used as piezoelectric material. The device is encapsulated in vacuum conditions by a top and bottom glass capping to limit fluidic damping mechanisms. When the package is excited by an external vibration, the beam is strained so that electrical charges develop at the surface of the piezoelectric layer. They are allowed to flow into an electrical load circuit connected via the contact pads.

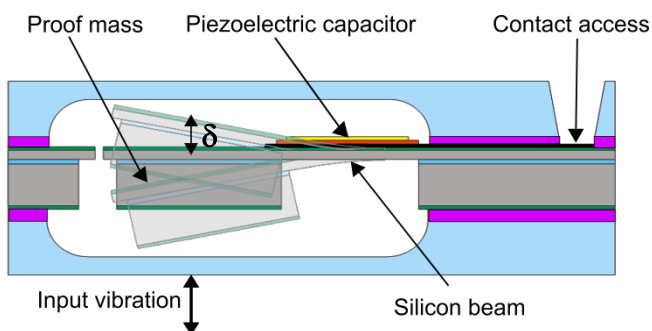


Fig.1: Schematics of the fabricated MEMS harvesters.

In the first section of the article, the method we developed for fabricating the PVEH is described. The characteristics of the devices obtained from an initial and refined version of the manufacturing method are compared. The refined version leads to a better yield and to devices with larger mechanical quality factor Q_m (due to a reduction of the parasitic damping) and effective electromechanical coupling K^2 [3] (due to a thicker piezoelectric layer). In the second section, the influence of Q_m and K^2 on the generated power is

analyzed from a theoretical point of view. Particularly, it is shown that a large Q_m leads to higher power per square unit input acceleration and a large electromechanical coupling leads to higher power per square unit displacement of the proof mass. In the third section, the theoretical predictions are confirmed by experimental measurements.

IMPROVED FABRICATION PROCESS

As shown in Figure 2, the devices are fabricated on 6 inch SOI wafers consisting of 50 μm $\langle 100 \rangle$ oriented silicon on top of 500 nm buried oxide and 625 μm silicon (Figure 2a). The top surface of the wafer is coated with 1 μm thermal compressive oxide (Figure 2b) which acts as a stress compensation layer for the piezoelectric capacitor deposited in the next steps. The piezoelectric capacitor is made of a MIM (metal-insulator-metal) stack consisting in 15 nm tantalum, 150 nm platinum, 2 μm aluminum nitride and 500 nm aluminum (Figure 2c). The shape of the capacitors is then defined by successive wet (AlN and Al) or dry (Pt) etching of the conductive and piezoelectric layers (Figure 2d). The next step involves dry etching of the thermal oxide and top silicon to define the outer boundaries of the oscillating device (Figure 2e). The proof mass and the cantilever are then obtained by dry etching of the bottom silicon (Figure 2f). The devices are released by buffered HF etching of the buried oxide (Figure 2g). Finally, the device wafer is vacuum encapsulated between a top and bottom glass wafer to obtain the system described in Figure 1. Devices with different dimensions are processed on the same wafer in order to target resonance frequencies ranging from 200 Hz to 1.2 kHz.

The 'yield' of the processed devices (defined here as the amount of PVEH exhibiting resonance frequency and capacitance in the desired range) reaches 95 %. This figure has to be compared with the 30% yield corresponding to our previous fabrication method [2].

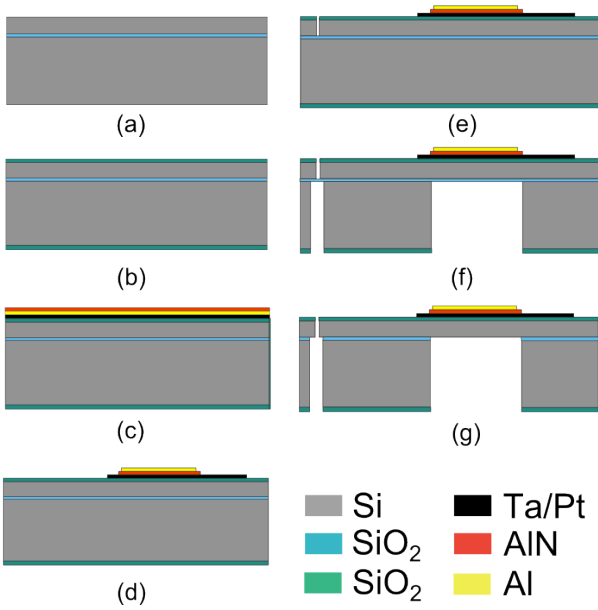


Fig.2: Fabrication process of the PVEH.

Two elements aimed at optimizing the performances in terms of energy harvesting of the fabricated PVEH are implemented in the current fabrication method. First, the vacuum level in the bonding chamber is reduced to 10^{-5} mbar which allows limiting the parasitic fluidic dissipations occurring in the devices. In terms of phenomenological parameters, this allows increasing the mechanical quality factor Q_m of the devices. Second, the thickness of the piezoelectric layer is increased from $1.2 \mu\text{m}$ to $2 \mu\text{m}$. This allows increasing the effective electromechanical coupling factor K^2 of the PVEH (a theoretical elaboration of the dependence of K^2 on the thickness of the piezoelectric layer can be found in [4]). As a matter of illustration, a comparison of the values of Q_m and K^2 measured on devices from the initial and refined fabrication methods are given in Table 1. The length of the silicon beam and proof mass are $1760 \mu\text{m}$ and $3000 \mu\text{m}$, respectively, while the width of the two elements is $3000 \mu\text{m}$. These devices are designed to resonate at about 1 kHz. It can be seen that the quality factor is doubled while the electromechanical coupling is increased by 35 %.

Table 1: Measured parameters for 7 devices of the previous and current fabrication method.

	$10^3 K^2$	Q_m
Current run	3.5 ± 0.3	2100 ± 200
Previous run	2.6 ± 0.2	1200 ± 200

Higher values of Q_m and K^2 have a positive influence on the power generated by the PVEH, as explained in the next sections.

THEORY

The model used to predict the performances of the PVEH has already been described in the literature [3] and details are not presented here. According to this model, the power delivered by a PVEH to a load resistor R can be written as Eq.1 in which A_0 and ω are respectively the amplitude and frequency of the input acceleration (assumed sinusoidal), m is the effective mass of the device, C_p the clamped capacitance and ω_0^R the fundamental resonance frequency of the PVEH (short circuit resonance frequency). Ω corresponds to the frequency of the input normalized to ω_0^R and Ψ is a normalized load parameter.

$$P = \frac{mA_0^2}{2\omega_0^R} \frac{\Omega^2 K^2 \Psi}{(\Omega^2 - 1)^2 + \Omega^2 \Psi^2 (\Omega^2 - 1 - K^2)^2 + D} \quad (1)$$

with

$$D = \frac{1}{Q_m} \left(\frac{1}{Q_m} + 2\Omega \Psi \left(K^2 + \frac{\Omega \Psi}{2Q_m} \right) \right) \quad (2)$$

$$\Omega = \frac{\omega}{\omega_0^R} \quad (3) \quad \Psi = RC_p \omega_0^R \quad (4)$$

The generated power is directly proportional to the effective mass and to the square of the input acceleration, while it is inversely proportional to ω_0^R . The influences of the input vibration frequency and load parameter are not so obvious. As shown in [3], the analysis of (1) reveals that a single maxima of the power in terms of Ψ and Ω is observed when $K^2 Q_m < 2$ while two maximums and a saddle point are found when $K^2 Q_m > 2$. This phenomenon can be explained as follow. Maximum power transfer between the PVEH and the load is achieved when their impedances are matched. For $K^2 Q_m < 2$, the imaginary part X of the electrical impedance $Z = T + jX$ of the PVEH remains always negative. As the impedance of the load resistor is purely real, it is then not possible to obtain complete matching between the PVEH and R . Maximum power is instead obtained when $|Z| = R$. This condition corresponds to a single set of values for Ω and Ψ , which explains the presence of a single maximum. For devices with $K^2 Q_m > 2$, X becomes positive in a small range of frequencies around the resonance and crosses the zero line for two frequencies $\Omega \approx 1 = \Omega_0^R$ and $\Omega \approx (1 + K^2)^{1/2} = \Omega_0^A$, which correspond to the resonance and anti resonance normalized frequencies of the PVEH, respectively. In this case, it is possible to achieve complete electrical impedance matching ($R = T$ and $0 = X$) with the resistive load. The two power peaks correspond to the two sets of values (Ω, Ψ) where this condition is met. It is shown in [3] that the load parameter leading to this situation is $(1 + K^4 Q_m^2)^{1/2}$ at resonance and $(1 + K^4 Q_m^2)^{1/2}$ at anti resonance.

An interesting aspect of the saddle point found at the coordinates $\Omega \approx (1+K^2/2)^{1/2} = \Omega_0^{\eta}$ and $\Psi = 1$ was highlighted by Pozzi [5]: the efficiency of the electromechanical energy conversion is maximized at this point. Maximum efficiency corresponds to the optimum power per square unit displacement of the PVEH relatively to the package. This consideration is important as the PVEH are always constrained by a maximum displacement imposed in our case by the glass cappings.

Approximated formulas of the power and deflection δ (at the center of the proof mass, see Figure 1) for the resonance, anti resonance and maximum efficiency conditions are given in Table 2. At resonance and anti resonance, the power and deflection have the same value. However, the optimum load parameter differs strongly for the two situations [3]. Because the optimum load is relatively small (large) at resonance (anti resonance), large electrical currents (voltages) are obtained at resonance (anti resonance). The power normalized to the square input acceleration generated in these situations is directly proportional to Q_m , so that the larger it is, the better is the ‘sensitivity’ of the PVEH. Using the median numerical values for the new generation devices given in Table 1 in the formulas of Table 2, it is found that P/A_0^2 at Ω_0^R or Ω_0^A is about 140% the value obtained in the maximum efficiency condition. This is confirmed experimentally in Figure 3b. However, for a same input acceleration, the deflection δ at Ω_0^R or Ω_0^A is more than twice the one at Ω_0^{η} . Therefore, the power normalized to the square unit deflection in the maximum efficiency condition is 360 % the one obtained at resonance or anti resonance. As can be derived from the formulas of Table 2, P/δ^2 is directly proportional to K^2 in the maximum efficiency situation, which explains the interest of making this parameter large.

Table 2: Formulas for the power and deflection at resonance, anti resonance and maximum efficiency. These formulas are only valid for devices respecting the conditions $K^2 Q_m > 2$ and $K^2 \ll 1$.

	Resonance & Anti resonance	Maximum efficiency
Power	$\frac{mA_0^2}{\omega_0^R} \frac{Q_m}{8}$	$\frac{mA_0^2}{\omega_0^R} \frac{Q_m^2 K^2}{(2 + K^2 Q_m)^2}$
Deflection	$\frac{A_0}{(\omega_0^R)^2} \frac{Q_m}{2}$	$\frac{A_0}{(\omega_0^R)^2} \frac{2Q_m}{2 + K^2 Q_m}$

In practice, the choice of working in a resonant/anti resonant or maximum efficiency condition should be done in the following way:

- For low amplitude input vibrations which do not result in large deflections of the

PVEH, one should opt for the best sensitivity option, i.e. resonance or anti resonance.

- At the opposite, if the input acceleration is large and that the power is limited because the PVEH reaches its maximum allowed displacement, one should implement the optimum efficiency option.

The considerations expressed in this section are illustrated by experimental results in the next part.

EXPERIMENTS

Two devices with the same dimensions but issued from the initial and refined fabrication methods are characterized. Their lumped parameters are summarized in Table 3. Both devices have the same effective mass but different resonance frequencies and capacitance due the thicker piezoelectric layer in the refined method. Also, as introduced previously, the quality factor and the effective electromechanical coupling are larger for the new generation device. For both devices, the amplitude of the deflection at the free end of the mass is limited to 600 μm by the package. This corresponds to $\delta = 400 \mu\text{m}$.

Table 3. Characteristics of the tested devices.

	New generation	Previous generation
m (mg)	14	14
ω_0^R (rad.s ⁻¹)	6321	6123
C_p (pF)	240	320
$10^3 K^2$ (-)	3.6	2.5
Q_m (-)	1900	1400

In order to determine the values of the load resistor and input frequency leading to the resonance, anti resonance and maximum efficiency conditions, we performed a first series of experiments in which the load resistor is set to a fixed value, while the frequency of the input vibration is swept and the resulting power monitored (Figure 3). This experiment is repeated for various values of the load resistor. For each value of the load resistor, the power at optimum frequency is then plotted as given in Figure 4. The load and input frequency conditions leading to the three characteristic situations are determined from Figure 3 and 4.

The power generated versus the input acceleration in resonance and maximum efficiency conditions is given in Figure 5 for the new generation device. Note that the anti resonance behavior was determined experimentally to be almost exactly similar to the resonance behavior so that the conclusions for resonance also apply to anti resonance. The calculated deflection of the device is also presented. For low input accelerations, the power generated at resonance increases with a rate of 47 $\mu\text{W}/\text{g}^2$ (versus 35 $\mu\text{W}/\text{g}^2$ for the previous generation device), which is advantageous

compared to the $32 \mu\text{W}/\text{g}^2$ obtained at maximum efficiency. However, in the former condition, the power saturates at about $140 \mu\text{W}$ for an acceleration of 2.5 g, as the deflection reaches its maximum allowed value. In the optimum efficiency case, the maximum deflection is reached at 4 g, where $450 \mu\text{W}$ are obtained. In this condition, the power per square unit deflection is maximized with a value of $2.9 \text{ nW}/\mu\text{m}^2$ (versus $2.1 \text{ nW}/\mu\text{m}^2$ for the previous generation device), compared to $0.9 \text{ nW}/\mu\text{m}^2$ at resonance.

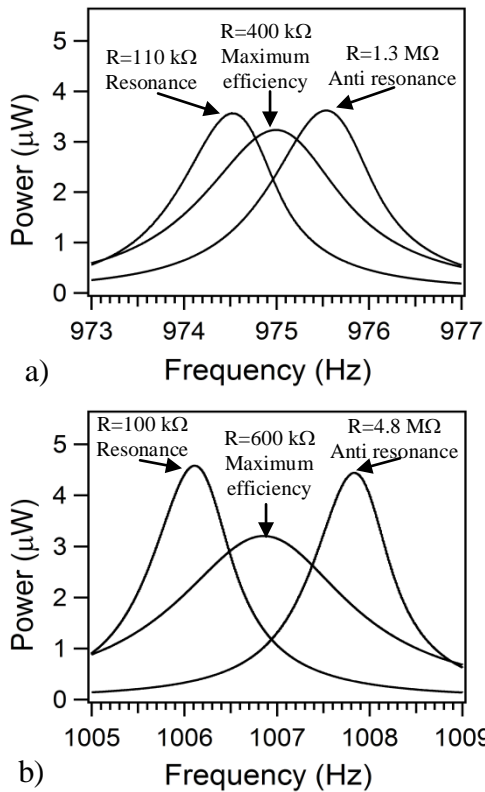


Fig.3: Experimental power vs. frequency generated by the previous (a) and new (b) generation device for an input acceleration amplitude of 0.32G .

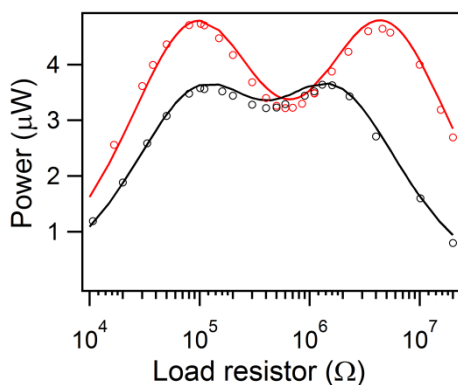


Fig.4: Power vs. the load resistor at optimum frequency for the previous (black color) and new (red color) generation devices for an input acceleration of 0.32G . The markers correspond to experiments and the solid lines to theoretical predictions.

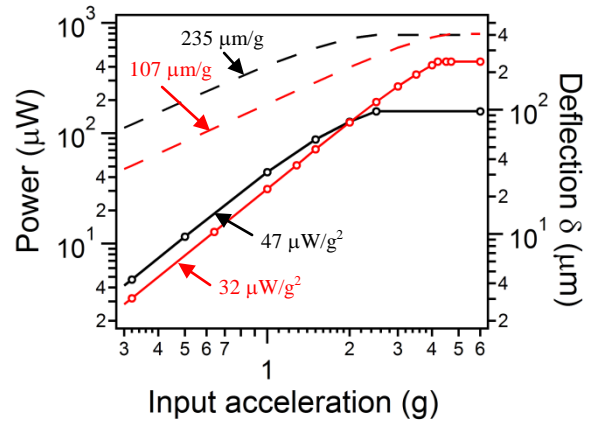


Fig.5. Power (solid lines) and deflection (dashed lines) vs. the input acceleration in resonance (black color) and maximum efficiency (red color) conditions. The markers correspond to experiments.

CONCLUSIONS

A reliable manufacturing process for MEMS piezoelectric vibration energy harvester is presented. Improvements of this process leading to a better yield of the fabricated devices and to better energy harvesting performances are discussed. Particularly, it is shown that a reduction of the parasitic losses lead to a better ‘sensitivity’ of the harvester, i.e. to enhanced values of the output power per square unit input acceleration. Also, it is demonstrated that, in our particular situation, increasing the thickness of the piezoelectric layer results in more efficient harvesters, i.e. to enhanced values of the output power per square unit deflection of the device. These elements are illustrated by both theoretical derivations and experimental measurements. Devices issued from our refined manufacturing method and resonating around 1 kHz generate up to $450 \mu\text{W}$ in optimum conditions.

REFERENCES

- [1] Akyildiz I F et al. 2002 Wireless Sensor Networks: A survey *Computer Networks* **38** (2002) 393–422.
- [2] Elfrink R et al. 2010 Vacuum Packaged Piezoelectric Vibration Energy Harvesters: Damping Contributions and Autonomy for a Wireless Sensor System *J. of Micromech. and Microeng.* **20** 1-7.
- [3] Renaud M et al. 2010 Power optimization using resonance and anti resonance characteristics of MEMS piezoelectric vibration energy harvesters *Proc. of Power MEMS 2010*.
- [4] Renaud M et al. 2007 Optimization of a piezoelectric unimorph for shock and impact energy harvesting *Smart Mat. Struct.* **16** 1125-1135
- [5] Pozzi M et al. 2011 Plucked piezoelectric bimorphs for knee joint energy harvesting: modeling and experimental validation, *Smart Mater. Struct.* **20**